

Article

High Sulfur Content of Mesoporous Activated Carbon Composite Derived from Water Hyacinth

Otong Nurhilal ^{1,2,*}, Suci Winarsih ² , Sahrul Hidayat ², Dadan Sumiarsa ³ and Risdiana Risdiana ^{2,*} 

- ¹ Study Program of Biotechnology, Postgraduate School, Universitas Padjadjaran, Jl. Dipatiukur No. 35, Bandung 40132, Indonesia
- ² Department of Physics, Faculty of Mathematics and Natural Sciences, Universitas Padjadjaran, Sumedang 45363, Indonesia; suciwinarsih93@gmail.com (S.W.); sahrul.hidayat@phys.unpad.ac.id (S.H.)
- ³ Department of Chemistry, Faculty of Mathematics and Natural Sciences, Universitas Padjadjaran, Sumedang 45363, Indonesia; dadan.sumiarsa@unpad.ac.id
- * Correspondence: otong.nurhilal@phys.unpad.ac.id (O.N.); risdiana@phys.unpad.ac.id (R.R.)

Abstract: Cathode composites with high sulfur content have become a concern to develop because they can improve the performance of lithium-sulfur batteries. The high sulfur content in the composite can be obtained from the carbon matrix, which has a high surface area and high electrical conductivity. Activated carbon made from biomass waste can be used as a carbon matrix due to its high surface area and ease of synthesis. In this study, activated carbon was prepared from water hyacinth (ACWH-600), which was carbonized at a temperature of 600 °C with a ZnCl₂ activator. Activated-carbon-sulfur composite (ACWH-600/S) was synthesized by mixing activated carbon and sulfur in a ratio of 1:3. The characterizations performed for ACWH-600 and ACWH-600/S were N₂ desorption-adsorption to determine the surface area, SEM to determine surface morphology, XRD to determine graphite structure, thermogravimetric analysis test to determine the sulfur content in the composite, and four-line probe conductivity to measure electrical conductivity at room temperature. The surface area, total pore volume, and pore diameter of ACWH were 642.39 m² g⁻¹, 0.714 cm³ g⁻¹, and 2.22 nm, respectively, while the surface area, total pore volume, and pore diameter of ACWH-600/S were 29.431 m² g⁻¹, 0.038 cm³ g⁻¹, and 2.54 nm. The conductivity value of ACWH-600 was 3.93 × 10⁻² S/cm, while for ACWH-600/S, the conductivity value was 2.24 × 10⁻⁴ S/cm. The decrease in conductivity value after activated carbon added sulfur indicated the success of synthesizing a carbon matrix from water hyacinth with high sulfur content. The high sulfur content of 58 wt%, together with the acceptable conductivity value of composite ACWH-600/S, provide an opportunity to apply these composites as cathodes in lithium-sulfur batteries.



Citation: Nurhilal, O.; Winarsih, S.; Hidayat, S.; Sumiarsa, D.; Risdiana, R. High Sulfur Content of Mesoporous Activated Carbon Composite Derived from Water Hyacinth. *Sustainability* **2021**, *13*, 12880. <https://doi.org/10.3390/su132212880>

Academic Editor: Mohammad Jafari

Received: 28 October 2021

Accepted: 17 November 2021

Published: 21 November 2021

Publisher's Note: MDPI stays neutral with regard to jurisdictional claims in published maps and institutional affiliations.



Copyright: © 2021 by the authors. Licensee MDPI, Basel, Switzerland. This article is an open access article distributed under the terms and conditions of the Creative Commons Attribution (CC BY) license (<https://creativecommons.org/licenses/by/4.0/>).

Keywords: activated carbon; water hyacinth; composite; conductivity

1. Introduction

In the last few years, lithium-sulfur batteries (LSB) have received significant attention from researchers. This is because the development of lithium-ion (Li-ion) batteries has experienced difficulties in increasing their capacity. It is difficult to achieve a specific capacity for lithium-ion batteries above 200 mA·h·g⁻¹. Even in the case of lithium cobalt oxide (LiCoO₂), which has a theoretical capacity of 274 mA·h·g⁻¹, only half of the Li-ions can be extracted because the other half is part of the matrix and total extraction of Li-ions results in lattice breakdown [1].

Theoretically, lithium metal has a specific capacity of 3861 mA·h·g⁻¹, and sulfur has a specific capacity of 1675 mA·h·g⁻¹. The theoretical specific energy density reaches 2600 Wh kg⁻¹, which is 3–5 times greater than conventional cathode materials such as LiCoO₂ and LiFePO₄ [2]. In addition, replacing conventional cathodes with sulfur has many advantages, including a low operating voltage (2.15 V vs. Li⁺/Li), which affects increasing its safety [3]. Sulfur is also a promising material because of its large reserves, low

cost, and being environmentally friendly compared to toxic transition metal compounds [4]. However, there are significant problems with the LSB cathode: first, sulfur is an insulator with a very low electrical conductivity value of 5×10^{-30} S/cm at 25 °C. Second, large volumetric expansion of sulfur occurs upon lithiation. Because of the density difference between sulfur and lithium sulfide (2.03 and 1.66 g/cm³, respectively), sulfur has a more significant volume expansion rate when it becomes lithium sulfide completely, which may lead to fracture and damage the electrode [5]. The strategy adopted to overcome the two problems at the cathode leads to modification of the carbon matrix for sulfur, which has high electrical conductivity, surface area, and pore volume. High electrical conductivity is required to increase the electrical contact of the sulfur. High surface area and pore volume are necessary to accommodate large amounts of sulfur.

The carbon matrix for sulfur can be in the form of micro, meso, and macroporous carbon, graphene [6], carbon nanotubes (CNT) [7], and also polymers [8]. Although significant improvements to battery performance stability have been achieved, the process of synthesizing carbon materials, such as graphite, graphene, CNT, and polymer, is high in cost [9]. Therefore, an effective and low-cost carbon matrix manufacturing strategy is needed to make a high-performance carbon matrix for sulfur.

Porous carbon materials derived from biomass have attracted increasing attention due to their abundance, sustainability, and easy accessibility [10]. Porous carbon from biomass is reported to have good electrical conductivity, a large specific surface area, and a large pore volume [11]. One of the porous carbons that have been developed is chemically activated carbon. This activated carbon is effective carbon matrix for sulfur and has good electrical contact between sulfur and carbon [12]. Activated carbon from biomass materials of bamboo [12], corn cobs [13], coconut shells [14], olive stones [15], banana peel [16], green algae [17], rapeseed shells [18], reed flowers [19], and water hyacinth (WH) [20] has been widely developed.

Among all the biomass materials used as activated carbon, WH is one biomass that needs to be studied intensively. This is because WH is invasive and has a high growth rate (60 kg/m²) [21], so WH will always be available in abundance, especially in tropical countries such as Indonesia. With its invasive nature and high growth rate, researchers have been trying to find ways to allow this WH to be used for various purposes. Several methods of utilizing WH have been reported, such as bioenergy (biogas, bioethanol, bio briquettes), phytoremediation, biofertilizers, high-value chemical products, animal feed, enzymes, biopolymers, and insulation boards in buildings [22].

WH has a biochemical component of 31.5% cellulose, 20.8% hemicellulose, and 21.3% lignin [23]. This high level of biochemical components is one of the advantages of WH, which can be used for the production of activated carbon. Activated carbon from WH has been reported as a substitute material for graphite in the active component of Li/Na-ion batteries [24]. However, activated carbon from WH as a component of the Li-S battery composite cathode has not been reported. Therefore, in this paper, we reported synthesis and characterization of activated carbon from WH (ACWH) and synthesis of the composite of ACWH with sulfur (ACWH/S), which can be developed as a cathode in Li-S batteries.

2. Materials and Methods

2.1. Synthesis of Activated Carbon

Water hyacinth has been collected from swamps in several cities in the Jawa Barat, Indonesia. ACWH was synthesized by simply carbonizing the water hyacinth as the precursor for carbon. After cleaning, the WH stems and leaves were taken and dried in the sun for 5–6 days, followed by an oven at 100 °C for 2 h. The dried water hyacinth was carbonized at 400 and 600 °C for 2 h at a heating rate of 10 °C/min in air and then cooled to room temperature naturally, resulting in a black powder. The carbon was then pulverized to a size of 200 mesh, then mixed with ZnCl₂ 30% (Sigma Aldrich, CAS Number: 7704-34-9) in the weight ratio of 1:3; then it was soaked for 24 h at room temperature and dried at 110 °C for 2 h and heated at 800 °C for 1 h with a heating rate of 10 °C/min under Ar flow.

Activated carbon samples from water hyacinth, which were carbonized at 400 and 600 °C, was coded ACWH-400 and ACWH-600, respectively.

2.2. Preparation of Activated Carbon-Sulfur Composite

Sulfur (Sigma Aldrich 99%, St. Louis, MO, USA) and the ACWH-600 sample were mixed with the weight ratio of 3.5:1 in a quartz mortar. The mixture was heated at 155 °C for 12 h to achieve the lowest viscosity of sulfur so that sulfur could easily enter the pores of the ACWH matrix.

2.3. Characterization

Characterization of the ACWH and ACWH/S composites were carried out by scanning electron microscopy (SEM, S-4800, Hitachi Limited, Tokyo, Japan), X-ray diffraction (XRD, Rigaku-TTRIII), Brunauer–Emmett–Teller (BET, Quantachrome Nova 4200e, Anton Paar, Graz, Austria), and Thermogravimetric analysis (TGA, Perkin Elmer TGA 4000, Waltham, MA, USA).

XRD patterns were determined by using Cu K α (wavelengths = 0.15418 nm) in the range of $10^\circ \leq 2\theta \leq 80^\circ$ (scan speed 5°/min and scan step 0.02°) at room temperature. Morphologies and microstructures of the samples were observed and analyzed by using the SEM operating at 10 kV. The sulfur content was detected using the TGA measurement under an air atmosphere, and the temperature range was from room temperature to 700 °C with a heating rate of 10 °C/min. Nitrogen sorption isotherms at 77 K were measured using the BET method.

2.4. Conductivity Measurement

The electrical conductivity measurements of both ACWH and ACWH/S samples were carried out using the four-line probe method at room temperature. A current variation of 0.01–0.05 mA from a DC source is applied to the two outer probes, and then the resulting voltage is measured at the two inner probes with a digital multimeter [25,26]. Based on the current and voltage curves, the resistivity and conductivity values can be determined. All samples were prepared in the form of a thin film. Each sample of 6.02 g was mixed with 0.25 g of carboxymethyl cellulose and 60.26 g of distilled water and stirred for 5 h with a magnetic stirrer at a temperature of 50 °C. Then, all solution samples are layered on top of the glass preparation until they reach a thickness between 100 and 300 μm .

3. Results and Discussion

The pore structure of the activated carbon samples was analyzed by the N₂ isotherm adsorption–desorption method. Figure 1a shows relative pressure (P/P_0) dependence of volume adsorbed for ACWH-400 (black circle for adsorption and purple circle for desorption) and ACWH-600 (blue circle for adsorption and red circle for desorption).

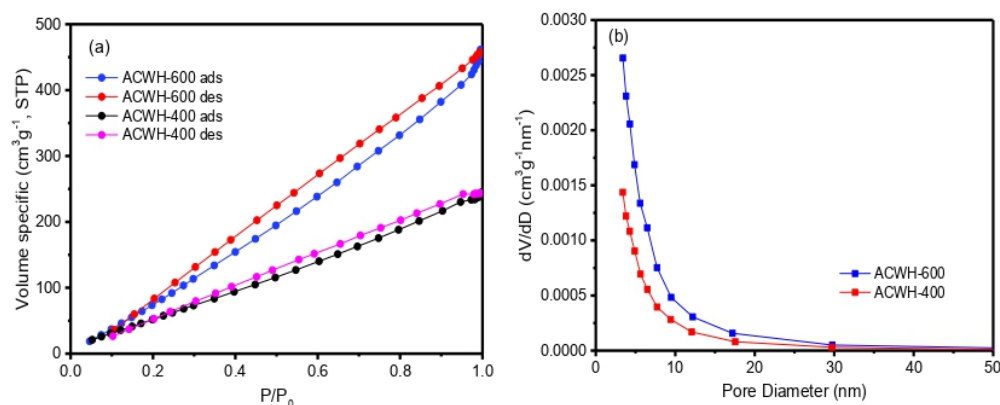


Figure 1. (a) N₂ adsorption–desorption isotherms of ACWH samples; (b) the Barrett–Joyner–Halenda method of pore size distribution curves from adsorption branch of ACWH samples.

It was found that the absorption of N_2 gas increased with increasing P/P_0 , and that desorption of N_2 gas decreased with decreasing P/P_0 for both samples. The values of volume adsorbed of ACWH-400 were smaller than those of ACWH-600, indicating that the carbonization process at a temperature of 600 °C produces more carbon than the carbonization process at a temperature of 400 °C. In both samples, hysteresis patterns were also found for the adsorption and desorption curves in the P/P_0 range between 0.2 and 0.9. Figure 1b shows the graph of pore diameter versus dV/dD based on the Barrett–Joyner–Halenda method. It is found that the pore size ranges are dominantly between 2 and 50 nm, which indicates that the sample is a mesoporous type [27].

The results of the N_2 gas isothermal adsorption–desorption test at a temperature of 77 K are listed in Table 1.

Table 1. Pore structure parameters of ACWH samples.

Sample	S_{BET} ($m^2 g^{-1}$)	V_{Meso} ($cm^3 g^{-1}$)	R_{Meso} (nm)
ACWH-400	297.76	0.378	2.54
ACWH-600	642.39	0.714	2.22

Based on Table 1, the quality of ACWH-600 is better than ACWH-400 with a larger surface area and total pore volume. The higher the carbonization temperature, the higher the fixed carbon content. The increasing of fixed carbon will increase the reaction between carbon and activator during the activation process.

The results of SEM measurements for the ACWH-600 sample and the ACWH-600/S composite are shown in Figure 2.

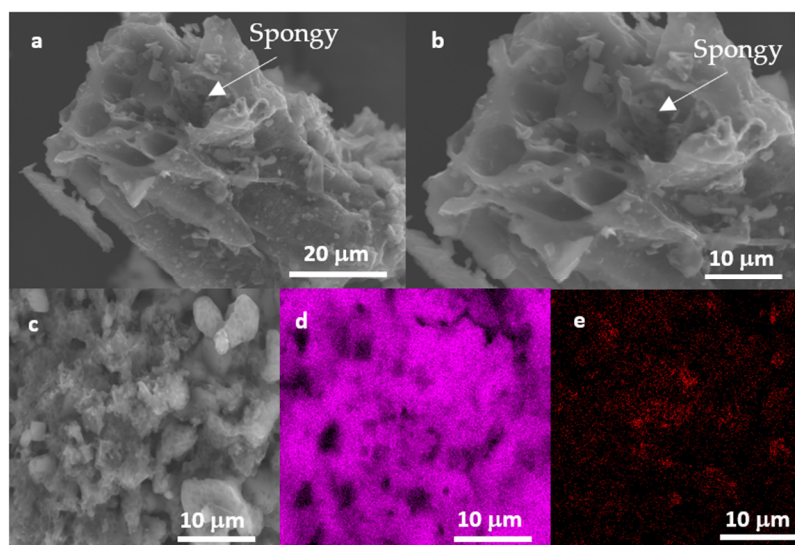


Figure 2. SEM, (a,b) ACWH600, (c) ACWH600/S, (d) Sulfur map, (e) Carbon map.

Figure 2a,b shows the particle size distribution of the ACWH-600 material. It can be seen that the surface of the ACWH-600 material is spongy. When the ACWH-600 material is composited with sulfur (ACWH-600/S), the surface of ACWH-600 becomes rougher because the sulfur particles gather and infiltrate the porous surface of ACWH-600, as shown in Figure 2c. Figure 2d,e shows a map of sulfur and carbon elements in the ACWH-600/S composite. The sulfur element map with purple color in Figure 2d is evenly distributed in the sample structure of ACWH-600/S. However, some parts on the surface of the ACWH-600/S sample are still not filled with sulfur, as shown by the black area. Meanwhile, the red map for element C (Figure 2e) shows that there is still element C that has not yet been composited with sulfur. Figure 2e indicates that the number of pores in element C filled with sulfur is still limited.

The N₂ gas isothermal adsorption test results at a temperature of 77 K ACWH-600 and composite ACWH-600/S are shown in Figure 3.

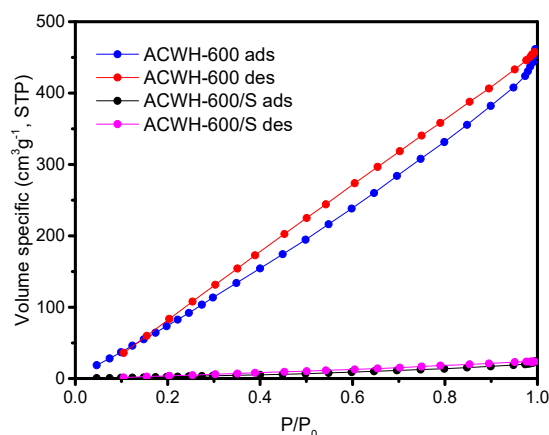


Figure 3. N₂ adsorption–desorption isotherms of ACWH-600 and ACWH-600/S.

The specific surface area and total pore volume of the composite were 29.431 m² g^{−1} and 0.038 cm³ g^{−1}, respectively. This indicates that the pores of ACWH-600 are already filled with sulfur. For applying cathode composites, the specific surface area and total pore volume values in this study met the requirements reported by Zhang et al. [28].

The XRD patterns for ACWH-600, sulfur (S), and ACWH-600/S composites are shown in Figure 4. All XRD data are matched with reference data with COD-CIF code No. 1000065 for graphite and COD-CIF No. 1011160 for sulfur. In Figure 4a, there are two main peaks observed in ACWH-600 at $2\theta = 28.3^\circ$, which characterizes the reflection of the vertical graphite plane (002), and at $2\theta = 40.5^\circ$, which indicates the superposition of the horizontal graphite plane (100). Figure 4b shows the crystal lattice peak at d-spacing of 0.385 nm, which corresponds to the plane (222) of elemental sulfur at $2\theta = 23.06^\circ$. The presence of peak (222) in the ACWH-600/S material indicates that sulfur has been successfully composited with ACWH-600. The TGA test results for ACWH-600 and composite ACWH-600/S are shown in Figure 5. For ACWH-600, the weight loss of activated carbon was almost constant up to 450 °C. Meanwhile, the sulfur weight loss was practically steady up to 350 °C, and then a drastic weight reduction occurred from 350 to 380 °C. In this temperature range, the sulfur absorbed is evaporated. From the sulfur weight reduction curve, it is estimated that the sulfur content in the composite is around 58 wt%. This result was proven by the N₂ isothermal test at a temperature of 77 K for the ACWH-600/S composite (Figure 3). There was a large difference between the specific surface area of activated carbon and composite.

The electrical conductivity measurement for ACWH-600 and ACWH-600/S with the FLP method obtained the average conductivity results of 3.93×10^{-2} S/cm and 2.24×10^{-4} S/cm, respectively. The conductivity of ACWH-600 is greater than the conductivity of WH charcoal, as measured by Azam et al., which is 1.64×10^{-5} S/cm [29]. While the conductivity of ACWH-600/S decreases, this indicates that the sulfur has mixed well in the carbon framework. When comparing the results of the electrical conductivity measurements for both ACWH-600 and ACWH-600/S with the crystal structures of these two materials, it was found that they agreed with the results of the crystal structure analysis obtained from XRD measurements as shown in Figure 4 and TGA measurements in Figure 5. The presence of sulfur, confirmed from the XRD and TGA measurements, caused a decrease in the conductivity value. However, this decrease in value is still within the range of the acceptable value for cathode applications in batteries. In addition, the results of this study also indicated the success of synthesizing a carbon matrix from WH with a high sulfur content and was a good sign for the development of battery material from abundantly available biomass, which will ensure the sustainability of its application.

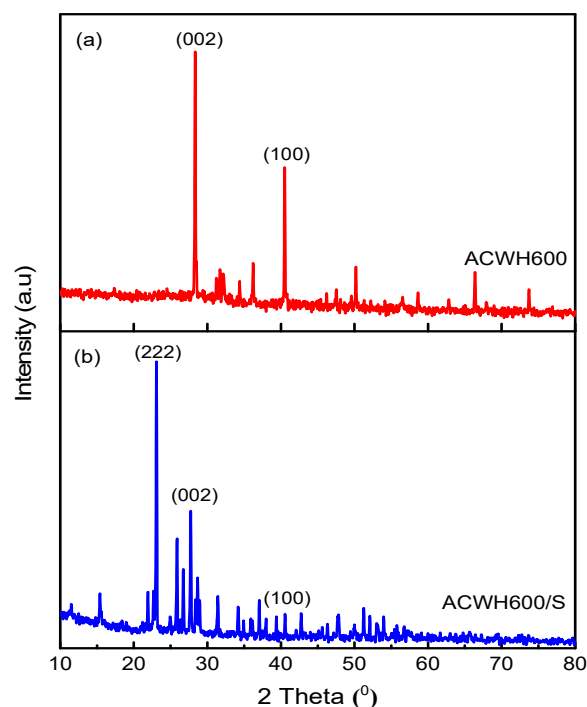


Figure 4. XRD pattern of (a) ACWH-600 and (b) composite ACWH-600/S.

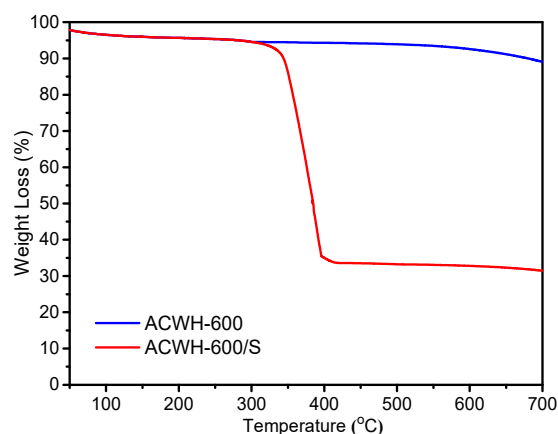


Figure 5. TGA curve for ACWH-600 and ACWH-600/S sample.

4. Conclusions

ACWH-600 and composite ACWH-600/S were successfully extracted from WH through carbonization and activation with ZnCl_2 . ACWH-600 and ACWH-600/S showed good properties for the application of cathode composites in lithium-sulfur batteries. The specific surface area of ACWH-600 was $642.39 \text{ m}^2 \text{ g}^{-1}$, the total pore volume was $0.714 \text{ cm}^3 \text{ g}^{-1}$, and the pore radius was 2.22 nm, which is sufficient to accommodate sulfur in the composite. XRD and TGA measurements confirmed that the ACWH-600/S composite was successfully synthesized with a high sulfur content of 58%. The conductivity value decreased after ACWH-600 was composited with sulfur from $3.93 \times 10^{-2} \text{ S/cm}$ to $2.24 \times 10^{-4} \text{ S/cm}$. This value is still in the range of acceptable values for cathode applications in batteries. These results indicate the success of synthesizing activated carbon from abundant biomass materials, namely WH, which can be used as a matrix for ACWH-600/S composites for cathode applications in the lithium-sulfur battery.

The following research plan is to scale up the synthesis of ACWH-600/S composites and manufacture lithium-sulfur batteries with cathodes derived from the ACWH-600/S

composites. These research activities are significant to fulfill the need for batteries, for which one of the components is derived from abundant biomass.

Author Contributions: Conceptualization, O.N. and R.R.; data curation O.N. and S.H.; formal analysis, O.N.; S.W. and D.S.; supervision, R.R.; writing—original draft preparation, O.N. All authors have read and agreed to the published version of the manuscript.

Funding: This research was funded by Universitas Padjadjaran. No. 1959/UN6.3.1/PT.00/2021.

Institutional Review Board Statement: Not applicable.

Informed Consent Statement: Not applicable.

Data Availability Statement: Not applicable.

Acknowledgments: These works are doctorate program research at a Postgraduate School in the Biotechnology Study Program at Universitas Padjadjaran and are financially supported by *Riset Disertasi Dosen Unpad* (RDDU) and the Academic Leadership Grant of Universitas Padjadjaran, No. 1959/UN6.3.1/PT.00/2021.

Conflicts of Interest: The authors declare no conflict of interest.

References

1. Eftekhari, A.; Kim, D.W. Cathode materials for lithium–sulfur batteries: A practical perspective. *J. Mater. Chem. A* **2017**, *5*, 17734–17776. [[CrossRef](#)]
2. Adelhelm, P.; Hartmann, P.; Bender, C.L.; Busche, M.; Eufinger, C.; Janek, J. From lithium to sodium: Cell chemistry of room temperature sodium–air and sodium–sulfur batteries. *Beilstein J. Nanotechnol.* **2015**, *6*, 1016–1055. [[CrossRef](#)]
3. Zhang, S.S. Liquid electrolyte lithium/sulfur battery: Fundamental chemistry, problems, and solutions. *J. Power Sources* **2013**, *231*, 153–162. [[CrossRef](#)]
4. Swiderska-Mocek, A.; Rudnicka, R. Lithium sulphur battery with activated carbon cloth-sulphur cathode and ionic liquid as electrolyte. *J. Power Sources* **2015**, *273*, 162–167. [[CrossRef](#)]
5. Liu, P.; Wang, Y.; Liu, J. Biomass-derived porous carbon materials for advanced lithium sulfur batteries. *J. Energy Chem.* **2019**, *34*, 171–185. [[CrossRef](#)]
6. Yuan, S.; Guo, Z.; Wang, L.; Hu, S.; Wang, Y.; Xia, Y. Leaf-like graphene-oxide-wrapped sulfur for high-performance lithium-sulfur battery. *Adv. Sci.* **2015**, *2*, 1500071. [[CrossRef](#)] [[PubMed](#)]
7. Yu, Y.; Luo, Y.; Wu, H.; Jiang, K.; Li, Q.; Fan, S.; Li, J.; Wang, J. Ultrastretchable carbon nanotube composite electrodes for flexible lithium-ion batteries. *Nanoscale* **2018**, *10*, 19972–19978. [[CrossRef](#)] [[PubMed](#)]
8. Huang, S.; Guan, R.; Wang, S.; Xiao, M.; Han, D.; Sun, L.; Meng, Y. Polymers for high performance Li-S batteries: Material selection and structure design. *Prog. Polym. Sci.* **2019**, *89*, 19–60. [[CrossRef](#)]
9. Gu, X.; Wang, Y.; Lai, C.; Qiu, J.; Li, S.; Hou, Y.; Martens, W.; Mahmood, N.; Zhang, S. Microporous bamboo biochar for lithium–sulfur batteries. *Nano Res.* **2015**, *8*, 129–139. [[CrossRef](#)]
10. De, S.; Balu, A.M.; Jan, C.; Waal, V.W.; Luque, R. Biomass-Derived Porous Carbon Materials: Synthesis and Catalytic Applications. *ChemCatChem* **2015**, *7*, 1608–1629. [[CrossRef](#)]
11. Yang, K.; Gao, Q.; Tan, Y.; Tian, W.; Zhu, L.; Yang, C. Microporous carbon derived from Apricot shell as cathode material for lithium–sulfur battery. *Microporous Mesoporous Mater.* **2014**, *204*, 235–241. [[CrossRef](#)]
12. Yan, Y.; Shi, M.; Wei, Y.; Zhao, C.; Carnie, M.; Yang, R.; Xu, Y. Process optimization for producing hierarchical porous bamboo derived carbon materials with ultrahigh specific surface area for lithium-sulfur batteries. *J. Alloys Compd.* **2018**, *738*, 16–24. [[CrossRef](#)]
13. Xu, Z.; Geng, Z.; Yi, G.; Chen, C.; Xue, M.; Li, B.; Zhang, C. Corn-cob-derived Porous Carbon as an Interlayer Coating to Improve the Performance of Lithium Sulphur Battery. *Int. J. Electrochem. Sci.* **2017**, *12*, 4515–4527. [[CrossRef](#)]
14. Chen, Z.H.; Du, X.L.; He, J.B.; Li, F.; Wang, Y.; Li, Y.L.; Li, B.; Xin, S. Porous coconut shell carbon offering high retention and deep lithiation of sulfur for Lithium–Sulfur batteries. *ACS Appl. Mater. Interfaces* **2017**, *9*, 33855–33862. [[CrossRef](#)] [[PubMed](#)]
15. Moreno, N.; Caballero, A.; Morales, J.; Rodríguez-Castell, E. Improved performance of electrodes based on carbonized olive stones/S composites by impregnating with mesoporous TiO₂ for advanced LiS batteries. *J. Power Sources* **2016**, *313*, 21–29. [[CrossRef](#)]
16. Li, F.; Qin, F.; Zhang, K.; Fang, J.; Lai, Y.; Li, J. Hierarchically porous carbon derived from banana peel for lithium sulfur battery with high areal and gravimetric sulfur loading. *J. Power Sources* **2017**, *362*, 160–167. [[CrossRef](#)]
17. Zhao, Y.; Zhang, X.; He, Y.; Liu, N.; Tan, T.; Liang, C. Biomass Derived Nitrogen-Doped Highly Porous Carbon Material with a Hierarchical Porous Structure for High-Performance Lithium/Sulfur Batteries. *Materials* **2017**, *10*, 1158. [[CrossRef](#)] [[PubMed](#)]
18. Zheng, M.; Hu, Q.; Zhang, S.; Tang, H.; Li, L.; Pang, H. Macroporous Activated Carbon Derived from Rapeseed Shell for Lithium–Sulfur Batteries. *Appl. Sci.* **2017**, *7*, 1036. [[CrossRef](#)]

19. Wang, Z.; Zhang, X.; Liu, X.; Zhang, Y.; Zhao, W.; Li, Y.; Qin, C.; Bakenov, Z. High specific surface area bimodal porous carbon derived from biomass reed flowers for high performance lithium-sulfur batteries. *J. Colloid Interface Sci.* **2020**, *569*, 22–33. [[CrossRef](#)]
20. Liang, J.; Tang, D.; Huang, L.; Chen, Y.; Ren, W.; Sun, J. High oxygen reduction reaction performance nitrogen-doped biochar cathode: A strategy for comprehensive utilizing nitrogen and carbon in water hyacinth. *Bioresour. Technol.* **2018**, *267*, 524–531. [[CrossRef](#)]
21. Sindhu, R.; Binod, P.; Pandey, A.; Madhavan, A.; Jose, A.A.; Narisetty, V.; Edgard, G.; Eulogio, C.; Vincenza, F. Water hyacinth a potential source for value addition: An overview. *Bioresour. Technol.* **2017**, *230*, 152–162. [[CrossRef](#)] [[PubMed](#)]
22. Ilo, O.P.; Simatele, M.D.; Nkomo, S.L.; Mkhize, N.M.; Prabhu, N.G. The Benefits of Water Hyacinth (*Eichhornia crassipes*) for Southern Africa: A Review. *Sustainability* **2020**, *12*, 9222. [[CrossRef](#)]
23. Rop, K.; Mbui, D.; Njomo, N.; Karuku, G.N.; Michira, I.; Ajayi, R.F. Biodegradable water hyacinth cellulose-graft-poly (ammonium acrylate-co-acrylic acid) polymer hydrogel for potential agricultural application. *Heliyon* **2019**, *5*, 01416. [[CrossRef](#)] [[PubMed](#)]
24. Zeng, G.; Zhou, B.; Yi, L.; Li, H.; Hu, X.; Li, Y. Green and facile fabrication of hierarchical N-doped porous carbon from water hyacinths for high performance lithium/sodium ion batteries. *Sustain. Energy Fuels* **2017**, *2*, 855–861. [[CrossRef](#)]
25. Flygare, J.D.; Riet, A.A.; Mazzeo, B.A.; Wheelera, D.R. Mathematical Model of Four-Line Probe to Determine Conductive Properties of Thin-Film Battery Electrodes. *J. Electrochem. Soc.* **2015**, *162*, A2136–A2144. [[CrossRef](#)]
26. Lanterman, B.J.; Riet, A.A.; Gates, N.S.; Flygare, J.D.; Cutler, A.D.; Vogel, J.E.; Wheeler, D.R.; Mazzeoa, B.A. Micro-Four-Line Probe to Measure Electronic Conductivity and Contact Resistance of Thin-Film Battery Electrodes. *J. Electrochem. Soc.* **2015**, *162*, A2145–A2151. [[CrossRef](#)]
27. Sotomayor, F.J.; Cychosz, K.A.; Thommes, M. Characterization of Micro/Mesoporous Materials by Physisorption: Concepts and Case Studies. *Acc. Mater. Surf. Res.* **2018**, *3*, 34–50.
28. Zhang, Y.; Zhao, Y.; Konarov, A.; Li, Z.; Chen, P. Effect of mesoporous carbon microtube prepared by carbonizing the poplar catkin on sulfur cathode performance in Li/S batteries. *J. Alloys Compd.* **2015**, *619*, 298–302. [[CrossRef](#)]
29. Imammuddin, A.M.; Soeparman, S.; Suprpto, W.; Sonief, A.A. Effect of Carbonization Temperature on Electrical Conductivity of Biocarbon Water Hyacinth Composites. *Int. J. Control Autom.* **2019**, *12*, 23–30. [[CrossRef](#)]